RENAL FAILURE
2025, VOL. 47, NO. 1, 2502875
https://doi.org/10.1080/0886022X.2025.2502875

Taylor & Francis
Taylor & Francis Group

LABORATORY STUDY

OPEN ACCESS Check for updates

Shen Shuai II Recipe alleviates renal fibrosis in chronic kidney disease by improving of hypoxia and inhibition of TLR4/MyD88/NF-κB/NLRP3 pathway

Yuan Zhou[a,b,c,d], Liang Zhou[a,b,c,d], Meng Wang[a,b,c,d], Lin Xu[a,b,c,d], Tingting Li[a,b,c,d] and Chen Wang[a,b,c,d]

[a]Department of Nephrology, Shuguang Hospital Affiliated to Shanghai University of Traditional Chinese Medicine, Shanghai, China; [b]Key Laboratory of Liver and Kidney Diseases, Ministry of Education, Shanghai University of Traditional Chinese Medicine, Shanghai, China; [c]TCM Institute of Kidney Disease, Shanghai University of Traditional Chinese Medicine, Shanghai, China; [d]Shanghai Key Laboratory of Traditional Chinese Clinical Medicine, Shanghai University of Traditional Chinese Medicine, Shanghai, China

ABSTRACT

Objectives: To investigate the anti-fibrotic mechanisms of Shen Shuai II Recipe (SSR) in chronic kidney disease (CKD), focusing on its modulation of hypoxia-associated inflammatory pathways and the TLR4/MyD88/NF-κB/NLRP3 axis

Methods: A 5/6 nephrectomy-induced chronic renal failure (CRF) rat model and hypoxia-exposed human renal tubular epithelial (HK-2) cells were utilized. In vivo, renal function was assessed via serum creatinine, urea nitrogen, and creatinine clearance measurements, alongside histopathological evaluation of renal fibrosis and inflammation. In vitro, hypoxia-treated HK-2 cells were analyzed for fibrotic markers (fibronectin, collagen I, α-smooth muscle actin) and pro-inflammatory cytokines (IL-1β, IL-18). Molecular mechanisms were probed through protein expression analysis of HIF-1α and the TLR4/MyD88/NF-κB pathway, with NLRP3 inflammasome activity evaluated.

Results: SSR treatment significantly improved renal function in CRF rats, reducing serum creatinine (Scr) and urea nitrogen (BUN) while enhancing creatinine clearance. Histopathology revealed preserved renal architecture with attenuated fibrosis and inflammatory infiltration. In hypoxic HK-2 cells, SSR downregulated fibrotic markers and suppressed IL-1β and IL-18 levels. Mechanistically, SSR reduced HIF-1α expression, inhibited TLR4/MyD88/NF-κB signaling, and suppressed NLRP3 inflammasome activation in both models.

Conclusions: SSR alleviates renal fibrosis and CKD progression by mitigating hypoxia-driven inflammation and blocking the TLR4/MyD88/NF-κB/NLRP3 pathway.

GRAPHICAL ABSTRACT

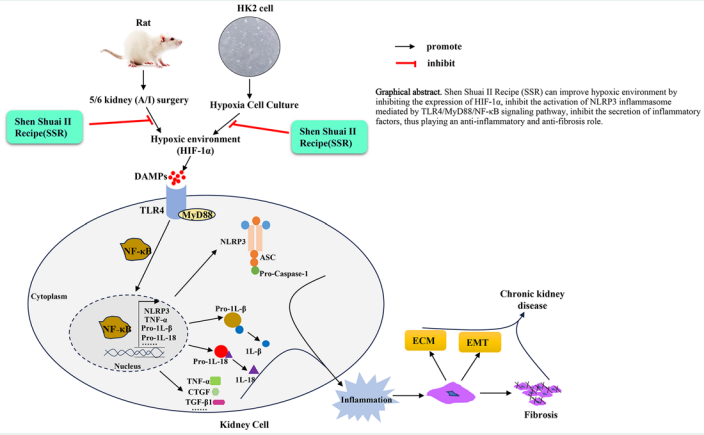

ARTICLE HISTORY

Received 10 January 2025
Revised 9 April 2025
Accepted 30 April 2025

KEYWORDS

Shen Shuai II Recipe (SSR); hypoxia; renal interstitial fibrosis; inflammation; TLR4/MyD88/NF-κB

CONTACT Yuan Zhou zhouyuan850722@163.com; Chen Wang chenwang42@126.com Department of Nephrology, Shuguang Hospital Affiliated to Shanghai University of Traditional Chinese Medicine, 528 Zhangheng Road, Pudong District, Shanghai 201203, China.
Yuan Zhou and Liang Zhou contributed equally to this work.

Supplemental data for this article can be accessed online at https://doi.org/10.1080/0886022X.2025.2502875.

Introduction

Chronic kidney disease (CKD) represents a global health burden, affecting millions worldwide and frequently progressing to end-stage renal disease (ESRD) with substantial morbidity and mortality [1–3]. Renal fibrosis, a hallmark pathological feature of CKD, arises from excessive extracellular matrix (ECM) deposition and serves as a critical determinant of ESRD progression [4]. Despite therapeutic advancements, the molecular mechanisms driving fibrotic pathogenesis remain incompletely elucidated, necessitating innovative therapeutic approaches.

Renal hypoxia is a critical driver of CKD progression, inducing epithelial-mesenchymal transition (EMT) in renal tubular cells, oxidative stress, fibroblast activation and immune-inflammatory responses, all contributing to renal function decline [5–7]. Notably, hypoxia develops early in CKD pathogenesis [8], while chronic inflammation exacerbates interstitial fibrosis through peritubular capillary rarefaction and impaired oxygen diffusion, establishing a self-perpetuating cycle of hypoxia-aggravated fibrosis [9]. Mechanistically, hypoxia-induced damage-associated molecular patterns (DAMPs) activate Toll-like receptor 4 (TLR4), which recruits myeloid differentiation primary response 88 (MyD88) to stimulate nuclear factor κB (NF-κB) signaling, this cascade drives proinflammatory cytokine transcription and activates the nucleotide-binding oligomedal-like receptor protein 3 (NLRP3) inflammasome, a pivotal mediator of inflammatory fibrosis [10,11]. Although TLR4's role in macrophage-mediated inflammation and lipopolysaccharide (LPS)-induced models is well-characterized [12], its activation in hypoxic renal tubular epithelial cells and subsequent inflammatory consequences remain underexplored.

Shen Shuai II Recipe (SSR), a traditional Chinese herbal formulation clinically validated for CKD management, demonstrates therapeutic efficacy through multiple mechanisms: ameliorating renal dysfunction [13,14], enhancing renal perfusion [15], and suppressing inflammatory mediators [5,16].

This study elucidates SSR's anti-inflammatory and anti-fibrotic mechanisms under hypoxic conditions through integrated *in vivo* and *in vitro* approaches. Focusing on hypoxia-induced inflammation mediated by the TLR4/MyD88/NF-κB signaling pathway and its role in renal interstitial fibrosis, we examined the expression of TLR4/MyD88/NF-κB and NLRP3 inflammasome pathway-related proteins in 5/6 nephrectomy (A/I) rat models and hypoxia-induced HK-2 cells. Employing pharmacological inhibition (MCC950, a selective NLRP3 inhibitor) and genetic silencing (MyD88 siRNA), we delineate SSR's dual role in improving hypoxia and suppressing TLR4/MyD88/NF-κB pathway, NLRP3 inflammasome activation and inflammatory factor secretion, thereby revealing its novel therapeutic mechanism against chronic renal fibrosis.

Materials and methods

Experimental animals

Male specific pathogen-free (SPF) Sprague Dawley rats (eight weeks old; 140–160 g body weight) were purchased from Shanghai Sipple-Bikai Laboratory Animal Co., LTD. (Animal License No. SCXK [Shanghai] 2012-0002) and housed in Laboratory Animal Center of Shanghai University of Traditional Chinese Medicine. Animals were maintained under controlled environmental conditions: 25 °C, 45% relative humidity, 12 h light/dark cycle, with *ad libitum* access to food and water, adaptive feeding for one week. This experiment was approved by the Ethics Committee of Shanghai University of Traditional Chinese Medicine, and the animal ethics registration number was No. SZY201604006. The experimental process strictly abides by the relevant national standards for the protection and use of experimental animals.

Experimental drugs and preparation

The composition of SSR was shown in Supplementary Table 1. The qualified raw herbs in SSR were from Shanghai Kangqiao Chinese Medicine Tablets Co., LTD. (Shanghai, China), with quality meeting the 2020 edition of Chinese Pharmacopeia. For cell experiments, the SSR aqueous extract (6 g/mL stock, prepared as described below) was diluted to working concentrations (400 μg/mL) using sterile DMEM/F12 medium. To ensure sterility, the diluted SSR solution was filtered through a 0.22 μm pore-size syringe filter (Millipore) before application to cell cultures. Losartan potassium (Merck Pharmaceutical Co., LTD.) was dissolved in sterile distilled water to a concentration of 5 mg/mL and similarly filtered., which was as positive controls.

SSR decoction was prepared by Shuguang Hospital affiliated to Shanghai University of Traditional Chinese Medicine. As we described earlier [17]. Briefly, Raw herbs and distilled water were mixed in a defined ratio, soaked for 1 h, and then decocted twice (30 min per cycle, high-to-low heat). The combined extracts were concentrated to 6 g/mL, aliquoted and stored at −80 °C.

Animal model

The rat model of chronic kidney disease was established *via* a two-stage 5/6 nephrectomy (ablation/infarction, A/I) procedure, as previously described [16]. First stage operation: After weighing the rats, 2% pentobarbital sodium was injected intraperitoneally at the dosage of 2 mL/kg for anesthesia. Rats were positioned in right lateral recumbency on a thermostatically controlled operating table, and a 2 cm transverse incision was made perpendicular to the spine below the left costal arch. The posterior and anterior descending branches of the left renal artery were ligated with non-absorbable silk sutures (4-0), inducing ischemic infarction of approximately two-thirds of the left renal parenchyma. This vascular ligation method achieves functional nephron reduction equivalent to physical resection while minimizing surgical trauma. Second stage operation: Seven days after the first surgery, rat was placed in the left lateral recumbency, and the right kidney was excised by ligating the renal artery, vein and ureter. Four weeks after second surgery, rats were randomly divided into three groups: 5/6 ablation and infarction (5/6 (A/I)) model group ($n=11$), 5/6 (A/I) + SSR group ($n=11$), 5/6 (A/I) +

Losartan group ($n = 11$). Next day, the corresponding intervention was given. The rats in sham operation group and model group were treated with 2 mL normal saline, 5/6 (A/I) + SSR group was given SSR (12 g, 2 mL), 5/6 (A/I) + Losartan group was given losartan potassium (10 mg, 2 mL) [14]. Interventions were administered daily for eight weeks. Sham-operated controls underwent identical abdominal incision and renal capsule dissection without vascular ligation or nephrectomy. At 30 days post-second surgery, 24 h urine was collected and recorded using metabolic cage. Terminal blood and kidney samples were obtained under pentobarbital anesthesia (40 mg/kg) after the eight-week intervention (Sample size was determined based on effect sizes observed in prior CKD studies and post-hoc power analysis confirmed >90% power for primary endpoints.).

Biochemical analysis

Renal function parameters assessed include serum creatinine (SCr), uric acid (UA), urea nitrogen (BUN) and creatinine clearance rate (CCr). Ccr (ml/min) = urine creatinine (including mol/L) x 24 h urine volume (mL)/serum creatinine (μmol/L)/1440 min. For each sample, 200 μL of urine was collected, and 24 h urine volumes were meticulously recorded to ensure accurate CCr calculations. All biochemical analyses were performed by the clinical laboratory of Shuguang Hospital Affiliated to Shanghai University of Traditional Chinese Medicine using BECKMAN AU5800 automatic biochemical analyzer and Beckman Coulter AU biochemical analyzer according to the inspection operation procedures.

Renal histopathology analysis

Kidney tissues were fixed in 4% paraformaldehyde for 24 h, dehydrated through a gradient alcohol (70% to 100%), cleared in xylene, and embedded in paraffin. Serial sections (3 μm thickness) were prepared using a rotary microtome, mounted onto glass slides, and dried at 60 °C until complete paraffin melting and moisture evaporation. Then hematoxylin-eosin (HE) staining, Masson staining, and Periodic Schiff (PAS) staining were performed.

HE staining

The paraffin sections were in xylene I and II (10 min each) and rehydrated through a descending ethanol series (100% ethanol ×2, 95% ethanol, 85% ethanol, 70% ethanol; 3 min each). After rehydration to water, sections were transferred to hematoxylin dye solution for 5 min. After hematoxylin staining, sections were rinsed under running water until nuclei displayed distinct blue coloration. Sections were then immersed in 0.5% aqueous eosin solution for 5 min, followed by thorough rinsing with deionized water to remove unbound dye; Then put in 70% ethanol, 85% ethanol for 3 min each, 95% ethanol, anhydrous ethanol for 5 min each. Subsequently, sections were cleared in xylene I and II (5 min each) and mounted with neutral resin for microscopic analysis.

Masson staining

The paraffin sections were in xylene I and II (10 min each) and rehydrated through a descending ethanol series (100% ethanol ×2, 95% ethanol, 85% ethanol, 70% ethanol; 3 min each). Fully hydrated sections were then transferred to 2.5% potassium dichromate solution for overnight soaking., Then washed with running water to remove excess dye, placed in iron hematoxylin dye solution for 3 min, rinsed with running water, differentiated with 1% hydrochloric acid alcohol for 5 s, and rinsed with running water. Then add Richun red acid fuchsin dye solution for 5–10 min, rinse with running water and put in 1% phosphomolybdate aqueous solution for 3–5 min, then re-dyed with aniline blue solution for 5 min, and then differentiated with 1% glacial acetic acid for 1 min. Excess dye was removed under running water. Sections were dehydrated through a graded ethanol series (70%, 85%, 95%, and absolute ethanol; 3–5 min per step), cleared in xylene I and II (5 min each), and mounted with neutral resin for microscopic evaluation.

PAS staining

The paraffin sections were in xylene I and II (10 min each) and rehydrated through a descending ethanol series (100% ethanol ×2, 95% ethanol, 85% ethanol, 70% ethanol; 3 min each). Rehydrated sections were transferred to 0.5% periodic acid solution for oxidation (10–15 min), and washed with running water. Sections were immersed in Schiff reagent under dark conditions at room temperature for 30–60 min, followed by a 10-min rinse in running water. Sections were counterstained with hematoxylin for 1 min and re-stained with nuclei, differentiated in 1% hydrochloric acid alcohol for 1 min, and reverted to blue by ammonia; Running water to remove excess dye. Then sections were dehydrated through a graded ethanol series (70% ethanol-3 min, 85% ethanol-3 min, 95% ethanol-5 min, absolute ethanol-5 min) and cleared in xylene I and II (5 min each), and mounted with neutral resin for microscopic evaluation.

Cell culture and RNA interference

Human renal proximal tubular epithelial cells (HK-2; ATCC) were maintained in DMEM/F12 medium (Gibco) supplemented with 10% fetal bovine serum (FBS, Gibco) at 37 °C and 5% CO_2. Culture medium was refreshed every two to three days. For hypoxic exposure, cells at 60% confluency were transferred to a tri-gas hypoxic chamber (1% O_2, 5% CO_2, 94% N_2).

MyD88-targeting siRNA (sense strand: 5′-GCCUGUCUCUGU UCUUGAATT-3′) was designed and synthesized by Shanghai Gemma Company. siRNA transfection was performed using the lipofectamine 3000 reagent according to the manufacturer's instructions. The cells were uniformly seeded into six-well plates (20–30% confluency) and cultured in a constant oxygen incubator. Transfection was performed when the cell fusion degree was 40%–45%. After 12 h incubation, transfected cells were replenished with fresh medium and subjected to normoxic (21% O_2) or hypoxia conditions for subsequent treatments.

Cell viability assay

According to the manufacturer, the activity of HK-2 cells was determined by CCK-8. Briefly, HK-2 cells were seeded into 96-well plate at a density of 1×10^4 cells/well and incubated overnight at 37 °C under 5% CO_2 at room temperature. Cells were serum-starved in DMEM/F12 (Gibco) supplemented with 0.5% FBS for 12 h. After starvation, the medium was replaced with fresh serum-free DMEM/F12 containing 400 μg/mL SSR. Following 24-h treatment, 10 μl CCK8 reagent was added to each well, and after incubation for 2 h, Absorbance was measured at 450 nm using multimode reader.

Cell immunofluorescence

HK-2 cells were collected to prepare cell suspension, and then seeded onto glass coverslips in six-well plates at a density of 5000 cells/well and cultured in 1.5 mL complete medium for 24 h. Cells were rinsed with PBS and fixed with 4% paraformaldehyde (400 μL/well; Sigma-Aldrich) for 30 min at room temperature. Then the paraformaldehyde was sucked up and rinsed with PBS. 1 mL Triton X-100 was added to each well, permeated the cells at room temperature for 20 min, absorbed and discarded the permeable solution. Then 1 mL 1% BSA sealing liquid was add to each hole and sealed it at room temperature for 60 min; 200 μl diluted primary antibody was added (dilution ratio 1:100 ~ 1:200) and incubated overnight at 4 °C; After three PBS washes, 200 μL of diluted fluorescent secondary antibody was added (dilution ratio 1:200), and incubated at room temperature without light for 60 min. PBS blackout rinse. Then cells were stained with DAPI (1 μg/mL; Sigma-Aldrich) for 5 min at room temperature. After rinsing with PBS blackout, fluorescence images were observed and collected under fluorescence microscope.

Western blot analysis

Proteins were extracted from residual kidney tissue or human renal tubular epithelial cells (HK2) cells with RIPA lysis buffer containing protease and phosphatase inhibitors, and quantified by BCA. After SDS-PAGE gel separation. All membranes were initially marked with BeyoColor ™ color pre-dyed protein ladders (6.5–270 KD, Beyotime). The protein was electro-transferred to PVDF membrane and incubated with 5% skim milk sealer for 1 h. PVDF membrane was treated with anti-HIF-1α(1:2000), anti-fibronectin (FN) (1:2000), anti-collagen I (Col-I) (1:2000), anti-Col-III(1:500), anti-α-SMA(1:1000), anti-E-cadherin(1:1000), anti-vimentin (1:1000), anti-CTGF(1:1000), anti-TGF-β1(1:2000), anti-p-NF-κB(1:1000), anti-NF-κB(1:1000), anti-TNF-α(1:1000), anti-MCP-1(1:100) 0), anti-interleukin (IL)-1β(1:1000), anti-IL-18(1:1000), anti-NLRP3(1:1000), anti-Caspase-1(1:2000), anti-pro-Caspase-1(1:2000), anti-ASC(1:1000), anti-TLR4(1:1000), anti-MyD88(1:2000), anti-GAPDH(1:2000) and anti-alpha-tubulin (1:2000) at 4°C overnight. The signal was detected by ECL method and quantified by Image J software.

Enzyme-linked immunosorbent assay (ELISA)

Cell culture supernatant (1 mL) was collected and centrifuged at 3000 × g for 20 min at 4 °C. Levels of IL-1β, Angiotensin II (AngII) and HMGB1 in the supernatant were quantified using ELISA kit (Shanghai, China) following the manufacturer's protocol.

Statistical analysis

Data were analyzed using SPSS 21.0 and GraphPad Prism 9.0. Continuous variables are presented as mean ± standard deviation. Parametric comparisons between two groups were performed using Student's t-test. For multi-group comparisons with normal distribution and homogeneous variance, one-way ANOVA was applied. Non-normally distributed data were analyzed using Kruskal–Wallis's test. Ordinal data were evaluated *via* Ridit analysis. Correlations among multiple variables were assessed through logistic regression and factorial analysis. A two-tailed $p < .05$ was considered statistically significant.

Results

Effect of SSR on renal function of in 5/6 nephrectomy (a/l) rats

Rats in the sham operation group exhibited normal behavior, responsiveness and healthy physical appearance, including smooth and glossy fur. In contrast, the 5/6 (A/I) model group displayed signs of illness, characterized by ruffled and discolored fur, lethargy, reduced food/water intake and impaired weight gain. Biochemical analysis revealed significant ($p < .01$) increases in serum creatinine (SCr) and BUN, accompanied by a reduction in endogenous CCr ($p < .01$). Both SSR- and losartan potassium-treated rats demonstrated significant improvements in dietary intake, hydration and weight gain compared to the untreated model group ($p < .01$). Furthermore, treatment with SSR or losartan potassium substantially reduced Scr ($p < .01$), BUN ($p < .01$) and UA ($p < .01$), while elevating CCr level ($p < .01$), No statistically significant difference were observed between SSR group and losartan potassium group (Table 1). These results indicate that SSR ameliorates renal dysfunction in chronic renal failure as well as losartan potassium.

Histopathological changes in 5/6(A/I)rats treated with SSR

HE staining showed that the sham-operated group exhibited intact glomerular morphology with normal cellularity and minimal inflammatory infiltration. In contrast, the 5/6 (A/I) model group severe structural disorganization, including disordered glomerular structure, blurred Bowman's capsule, balloon adhesions and multifocal inflammatory cell infiltration. Compared to the 5/6 (A/I) group, both SSR- and losartan potassium-treated groups showed significant improvements: glomerular structure was partially restored ($p < .01$), cell proliferation was reduced, Bowman's capsule integrity was preserved ($p < .01$) and interstitial inflammatory was reduced to focal infiltrates ($p < .01$) (Figure 1(A)). Masson's trichrome staining indicated minimal collagen deposition in the renal interstitium of the sham operation group. However, the 5/6 (A/I) model group displayed

Table 1. Comparison of renal function in all groups (x ± s).

Group	n	Scr/μmol/L	BUN/mmol/L	UA/μmol/L	Ccr/mL/min
Sham operation group	10	29.44 ± 3.68	6.13 ± 1.17	99.40 ± 16.27	2.13 ± 0.46
5/6(A/I) group	11	53.20 ± 2.49	11.04 ± 1.28	139.7 ± 12.16	1.30 ± 0.25
SSR group	11	43.00 ± 2.35**	8.63 ± 1.41**	110.3 ± 13.94**	2.12 ± 0.24**
Losartan potassium group	11	44.00 ± 2.74**	9.09 ± 1.04**	105.6 ± 12.52**	2.00 ± 0.10**
F		71.97	25.25	10.80	9.47
p		<.0001	<.0001	.0002	.0004

Note: '*' Compared with 5/6(A/I) group,
*$p < .05$,
**$p < .01$.

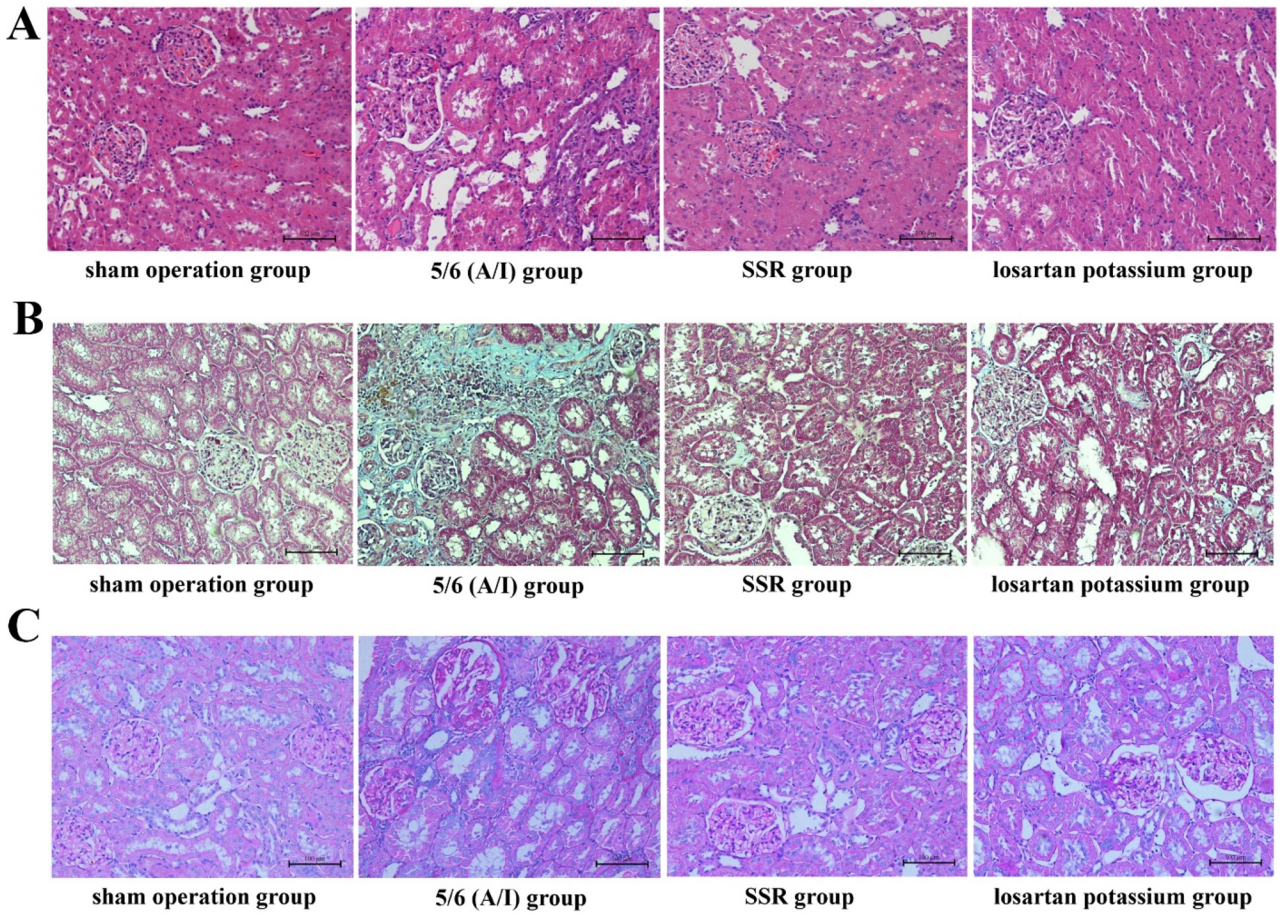

Figure 1. Histopathological evaluation of renal tissue in 5/6(a/I) rats treated with Shen Shuai II Recipe (SSR). (A) Comparison of hematoxylin-eosin (HE) staining results in renal tissue of rats in each group (×200). Sham-operated controls show intact glomerular architecture, while 5/6(a/I) rats exhibit structural disorganization, Bowman's capsule adhesions and interstitial inflammation. SSR-treated groups demonstrate preserved glomerular morphology and reduced inflammatory infiltration. (B) Masson's trichrome staining (×200) illustrating collagen deposition (blue) in renal interstitium. The 5/6(a/I) model displays extensive fibrosis, whereas SSR intervention attenuates collagen accumulation. (C) PAS staining (×200) reveals glomerular basement membrane integrity. Pathological features (thickened membranes, capillary collapse) in 5/6(a/I) rats are mitigated by SSR treatment. 5/6(a/I): 5/6 ablation and infarction.

extensive collagen fiber deposition in the renal interstitium ($p < .01$), indicative of advanced fibrosis. In comparison, both the SSR and losartan potassium treatments markedly attenuated collagen f accumulation ($p < .01$) (Figure 1(B)), with intergroup ANOVA confirming robust statistical significance ($F = 316.6$, $p < .001$). PAS staining further verified the above results. The sham operation group demonstrated normal glomerular basement membrane (GBM) thickness without mesangial hyperplasia or capillary collapse. In contrast, the 5/6 (A/I) model group, GBM thickening, capillary collapse, mesangial matrix expansion and interstitial inflammatory were prominent. Although residual pathological changes persisted in SSR- and losartan potassium-treated groups, tubule injury and inflammatory infiltration were significantly alleviated compared to the model group (Figure 1(C)).

Effects of hypoxia on fibrosis and inflammatory responses in HK-2 cells

Western blot analysis revealed that a significant upregulation of hypoxia-inducible factor-1α (HIF-1α) expression in HK-2 cells under hypoxic conditions compared to normoxia

compared to normoxia ($p < .01$, at all-time points: 12 h, 24 h, 36 h, 48 h, 72 h). HIF-1α expression levels peaked at 12 h of hypoxia and exhibited a time-dependent progression ($F = 15.59$, $p < .0001$; Figure 2(A,B)). Concurrently, CCK-8 assays revealed hypoxia-induced suppression of HK-2 cell viability over time ($F = 58.598$, $p < .001$, $\eta^2 = 0.527$; Figure 2(C)). Fibrosis-related markers, including FN, α-SMA, Col-I, CTGF and TGF-β1, were significantly upregulated in hypoxic HK-2 cells ($p < .01$), with expression intensities escalating with prolonged hypoxia ($p < .01$) (Figures 2(D–H) and 3(A,C,D)). Conversely, the expression of E-cadherin, an epithelial marker, exhibited a progressive decline under hypoxia ($F = 7.498$, $p < .001$; Figure 3(A,B)) while immunofluorescence confirmed hypoxia-induced fibrosis and EMT, characterized by increased α-SMA and diminished E-cadherin (Figures 3(E) and 4(A)). Hypoxia also significantly induced inflammatory responses in HK-2 cells. Western Blot analysis showed that p-NF-κB, TNF-α, MCP-1, IL-1β and IL-18 were markedly upregulated in hypoxic HK-2 cells ($p < .01$), with levels rising over time (Figure 4(B–G)). MCP-1 and IL-18 expression peaked at 36 h before declining ($p < .01$). ELISA results further confirmed hypoxia-induced elevations in HMGB1($p < .01$), Ang II ($p < .01$) and IL-1β ($p < .01$) in cell supernatants, mirroring HIF-1α dynamics (Figure 4(H–J)). ANOVA confirmed significant intergroup differences in inflammatory marker expression ($p < .05$). These data collectively establish hypoxia as a dual driver of fibrotic remodeling and inflammatory remodeling in HK-2 cells.

SSR modulates hypoxia, fibrotic response and inflammatory response in 5/6 (a/l) rats and hypoxic HK2 cells

In the 5/6 nephrectomy (A/I) rat model, renal hypoxia was confirmed by elevated HIF-1α expression ($p < .01$). SSR treatment significantly reduced HIF-1α levels ($F = 23.6$,

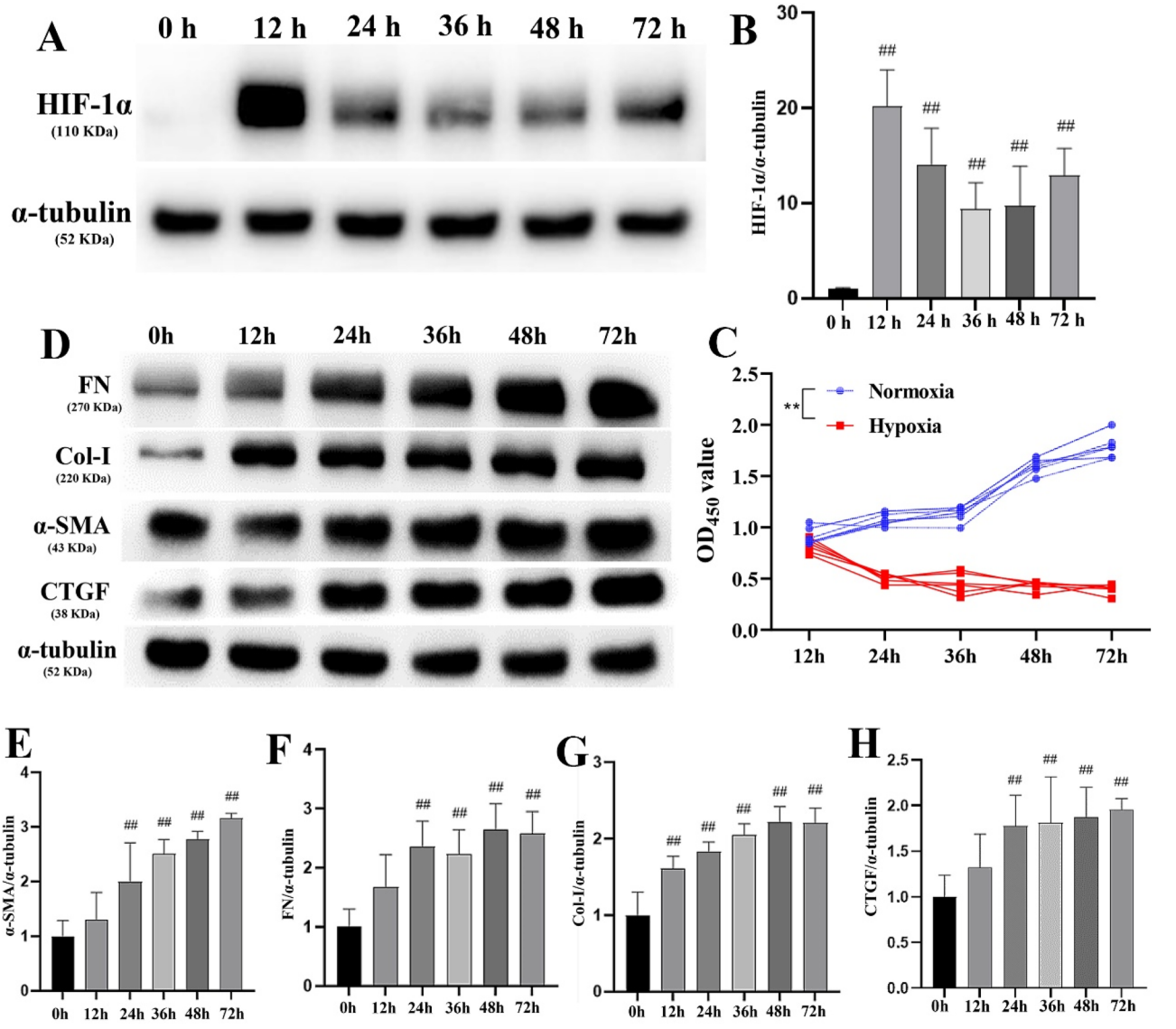

Figure 2. Hypoxia-induced fibrotic responses in HK-2 cells. (A,B) Western blot results of the effect of HIF-1α protein expression in hypoxia HK-2 cells. #: Compared with the 0 h group, ##$p < .01$. Protein bands: HIF-1α (1:2000, 110 KDa), α-tubulin (1:2000, 52 KDa). (C) CCK8 assay revealed progressive hypoxia-induced suppression of HK-2 cell viability. ** $p < .01$. (D) to (H) Western blot results of the effect of FN, Col-I, CTGF and α-SMA protein expression in hypoxia HK-2 cells. #: Compared with the 0 h group, ##$p < .01$. Protein bands: FN (1:2000, 270 KDa), Col-I (1:2000, 220KDa), α-SMA (1:1000, 43 KDa), CTGF (1:1000, 38 KDa), α-tubulin(1:2000, 52 KDa).

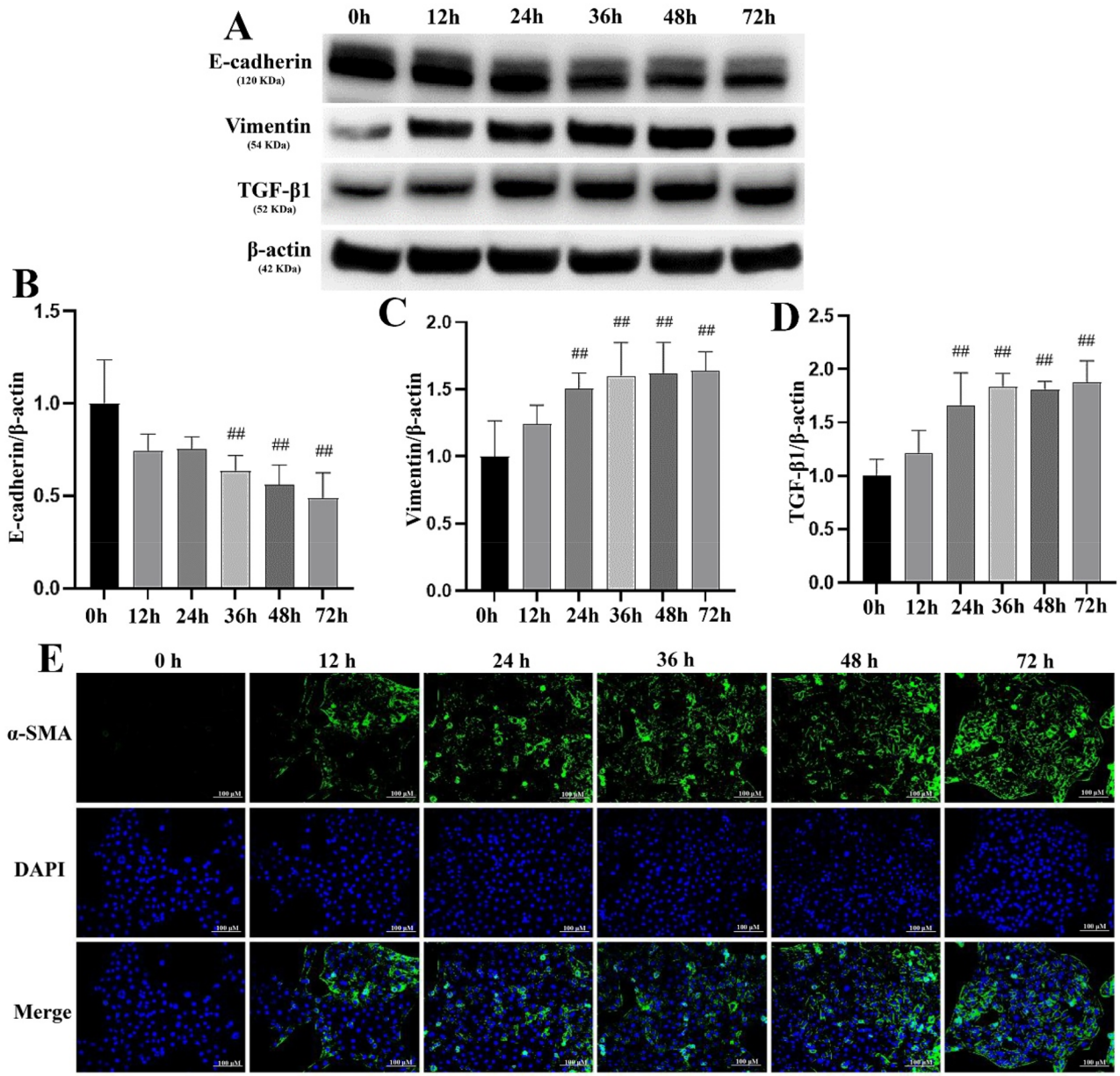

Figure 3. Hypoxia induces epithelial-mesenchymal transition (EMT) and fibrotic activation in HK-2 cells. (A) to (D) Western blot results of the effect of E-cadherin, vimentin, and TGF-β1 protein expression in hypoxia HK-2 cells. #: Compared with the 0 h group, ##$p < .01$. Protein bands: E-cadherin (1:1000, 120 KDa), vimentin (1:1000, 54 KDa), TGF-β1 (1:2000, 52 KDa), β-actin (1:2000, 42 KDa). (E) Immunofluorescence staining of α-SMA (green) and DAPI (blue) in HK-2 cells under hypoxia. Scale bar: 100 μm.

$p < .0001$), demonstrating its capacity to ameliorate hypoxia (Figure 5(A,B)). Furthermore, SSR intervention markedly decreased the expression of fibrotic markers, including FN ($p < .001$), Col-III ($p < .001$), Col-I ($p < .001$) and α-SMA ($p < .001$) in renal tissue (Figure 5(C–G)), suggesting that SSR suppresses myofibroblast activation and ECM deposition. Additionally, SSR attenuated EMT, marked by increased E-cadherin and reduced vimentin expression compared to the 5/6 (A/I) model group ($F = 23.18$, $p < .0001$) (Figure 5(H–J)). Furthermore, SSR exerted anti-inflammatory effects by suppressing NLRP3 inflammasome activation and downregulating inflammatory cytokines, including IL-1β and IL-18. Compared to the 5/6 (A/I) model group, SSR significantly reduced the expression of NLRP3($F = 8.726$, $p < .01$), pro-caspase-1($F = 18.02$, $p < .0001$), caspase-1($F = 14.1$, $p < .001$), apoptosis-associated speck-like protein containing a CARD (ASC) ($F = 9.567$, $p < .01$), IL-1β ($F = 7.603$, $p < .01$), and IL-18 ($F = 19.51$, $p < .0001$) in renal tissue (Figures 5(K,L) and 6(A–E)), highlighting its role in attenuating inflammation.

In hypoxic HK-2 cells, SSR (at concentrations ≤ 400 μg/mL for 24 h, as determined by CCK-8 assays; Supplementary Figure 1) consistently reduced HIF-1α expression ($F = 13.21$, $p < .0001$) and suppressed fibrotic markers (FN, α-SMA, and Col-I; $p < .01$) (Figure 6(F–K)), further confirming its ability to improve the hypoxic microenvironment and inhibit

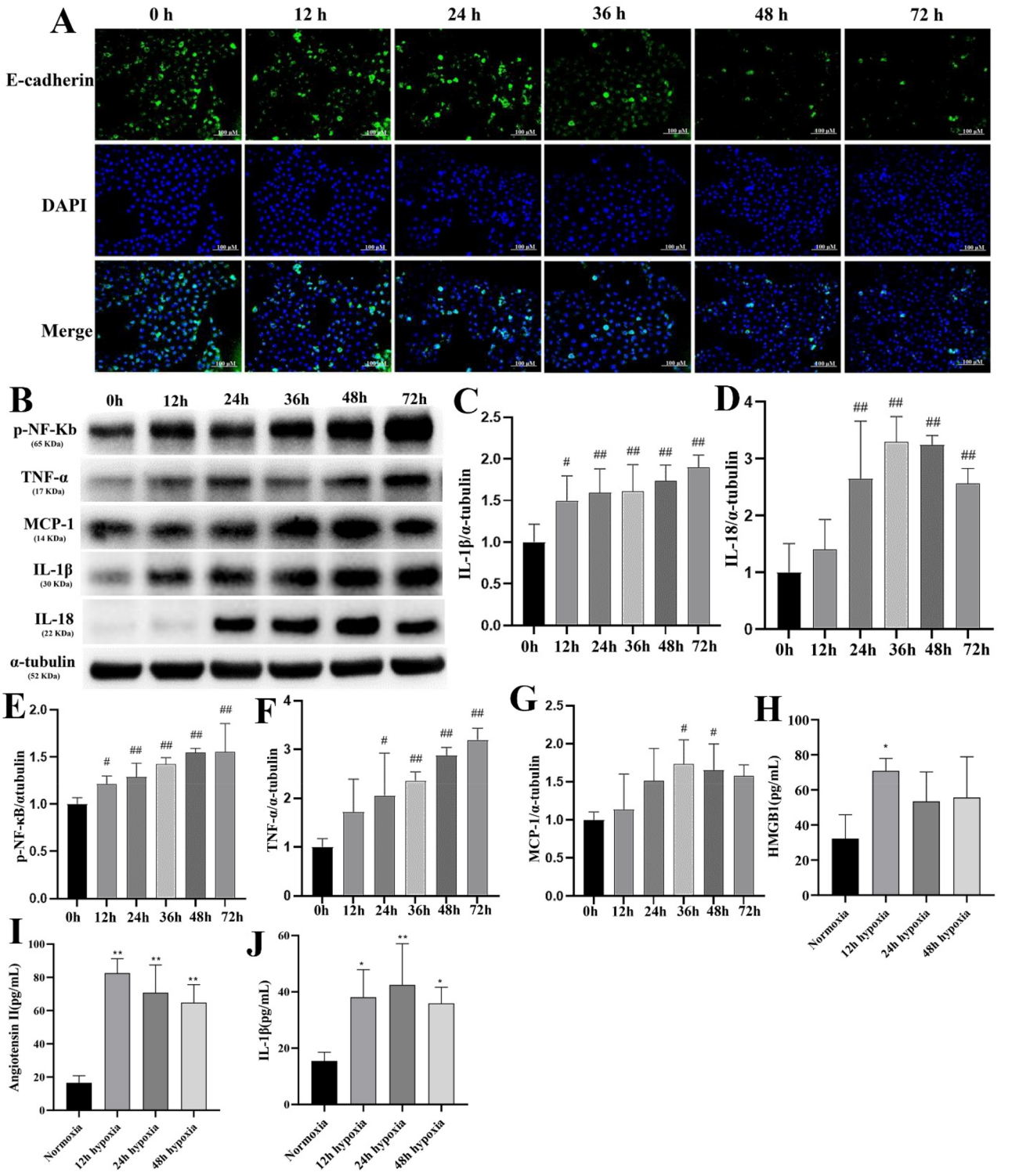

Figure 4. Hypoxia-induced inflammatory activation in HK-2 cells. (A) Immunofluorescence staining of E-cadherin (green) and DAPI (blue) in HK-2 cells under hypoxia. Scale bar: 100 μm. (B) to (G) Western blot results of the effect of inflammatory factor protein expression in hypoxia HK-2 cells. #: Compared with the 0 h group, #$p < .05$, ##$p < .01$. Protein bands: P-NF-κB (1:1000, 65 KDa), TNF-α (1:1000, 17 KDa), MCP1 (1:1000, 14 KDa), IL-1β (1:1000, 30 KDa), IL-18 (1:1000, 22 KDa), α-tubulin(1:2000, 52 KDa). (H) The levels of HMGB1 in the culture medium of hypoxia HK-2 cells. *$p < .05$. (I) The levels of Ang-II in the culture medium of hypoxia HK-2 cells. **$p < .01$. (J) The levels of IL-1β in the culture medium of hypoxia HK-2 cells. *$p < .05$, **$p < .01$.

fibrosis. Similarly, SSR also inhibited inflammatory signaling by decreasing the expression of p-NF-κB ($F = 12.70$, $p < .0001$), IL-1β ($F = 4.003$, $p < .05$) and IL-18 ($F = 6.246$, $p < .01$) (Figures 6(L) and 7(A–C)). ELISA revealed that SSR reduced the levels of IL-1β ($F = 6.094$, $p < .01$), HMGB1 ($F = 6.662$, $p < .01$) and Ang II ($F = 17.70$, $p < .0001$) in the cell supernatant (Figure 7(D–F)), further validating its anti-inflammatory effects.

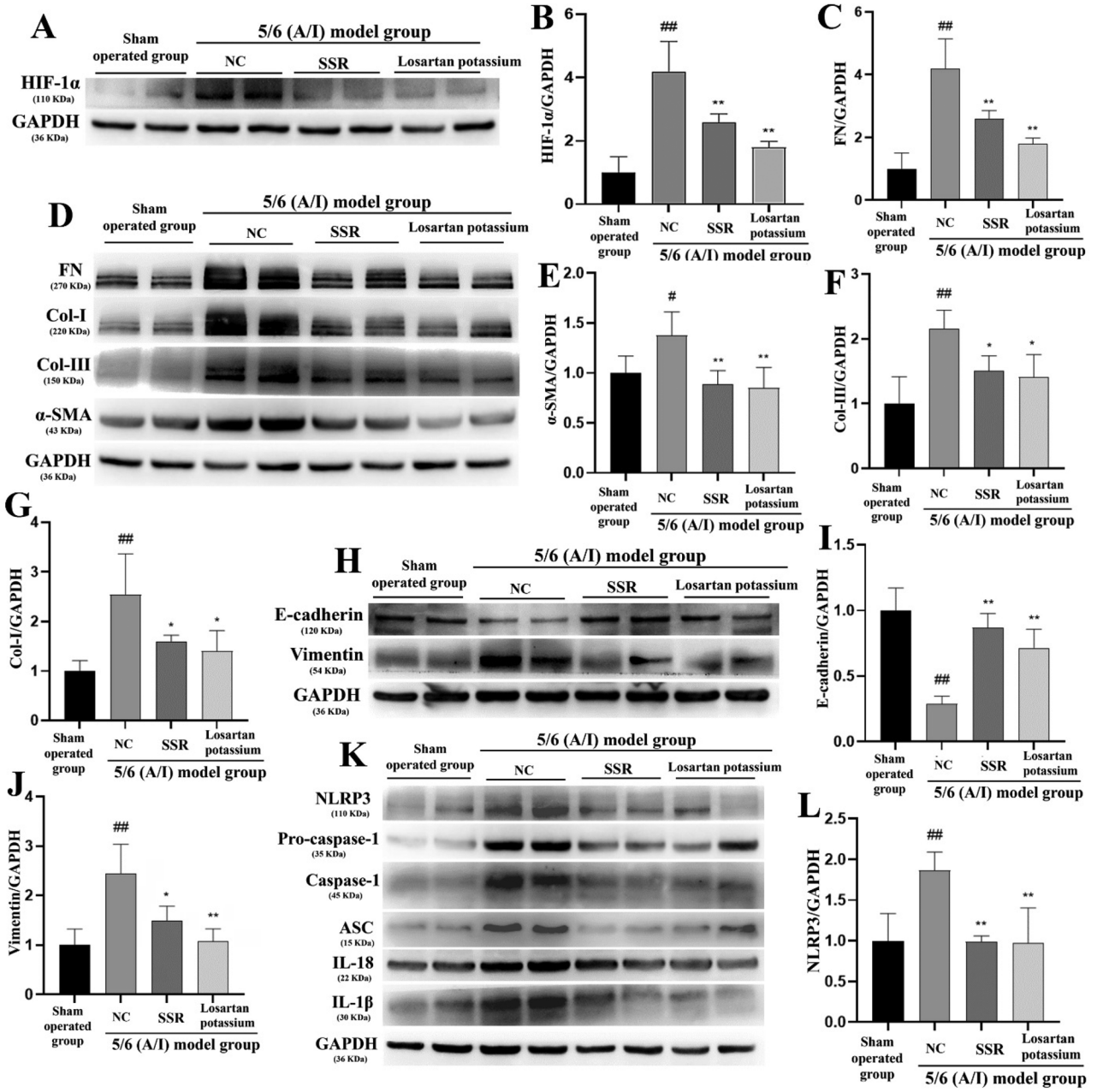

Figure 5. Shen Shuai II Recipe (SSR) attenuates hypoxia-driven fibrosis and NLRP3 inflammasome activation in 5/6 (A/I) rats. (A,B) Western blot results of the effect of SSR on the expression of HIF-1α in 5/6 (A/I) rats. #Compared with the sham-operated group, ##$p < .01$.*: Compared with the NC group, **$p < .01$. Protein bands: HIF-1α (1:2000, 110 KDa), GAPDH (1:2000, 36 KDa). (C) to (G) Western blot results of the effect of SSR on the expression of FN, Col-III, Col-I, and α-SMA in 5/6 (A/I) rats. #: Compared with the sham-operated group, #$p < .05$, ##$p < .01$.*: Compared with the NC group, *$p < .05$, **$p < .01$. Protein bands: FN (1:2000, 270 KDa), Col-I (1:2000, 220 KDa), α-SMA (1:1000, 43 KDa), Col-III (1:500, 150 KDa), GAPDH (1:2000, 36 KDa). (H) to (J) Western blot results of the effect of SSR on the expression of E-cadherin and vimentin in 5/6 (A/I) rats. #: Compared with the sham-operated group, ##$p < .01$.*: Compared with the NC group, *$p < .05$, **$p < .01$. Protein bands: E-cadherin (1:1000, 120KDa), vimentin (1:1000, 54 KDa), GAPDH (1:2000, 36 KDa). (K) and (L) Western blot results of the effect of SSR on the expression of NLRP3, pro-caspase-1, caspase-1, ASC, IL-1β, and IL-18 in 5/6 (A/I) rats. #: Compared with the sham-operated group, ##$p < .01$.*: Compared with the NC group, **$p < .01$. 5/6(a/I): 5/6 ablation and infarction.NC: negative control. Protein bands: NLRP3 (1:1000, 110 KDa), pro-caspase-1 (1:2000, 35 KDa), caspase-1 (1:2000, 45 KDa), ASC (1:1000,15KDa), IL-1β (1:1000, 30KDa), IL-18 (1:1000, 22KDa), GAPDH (1:2000,36KDa).

SSR attenuates hypoxia-induced HK-2 cell fibrosis via NLRP3 inflammasome inhibition

To elucidate the mechanistic role of the NLRP3 inflammasome in SSR's anti-fibrotic activity, we combined SSR with MCC950, a selective NLRP3 inflammasome inhibitor, in hypoxic HK-2 cells. Compared to the hypoxia group, both SSR and MCC950 significantly reduced the expression of HIF-1α, NLRP3, caspase-1, ASC, IL-1β, IL-18, Col-I, FN and α-SMA in HK-2 cells ($p < .01$ or $p < .05$). These findings demonstrate that SSR inhibits its NLRP3 inflammasome activation, consistent with its effects in the 5/6 nephrectomy (A/I) rat model, and confirm that NLRP3 inflammasome inhibition alleviates hypoxia-induced fibrosis in HK-2 cells. Notably, combined SSR and MCC950

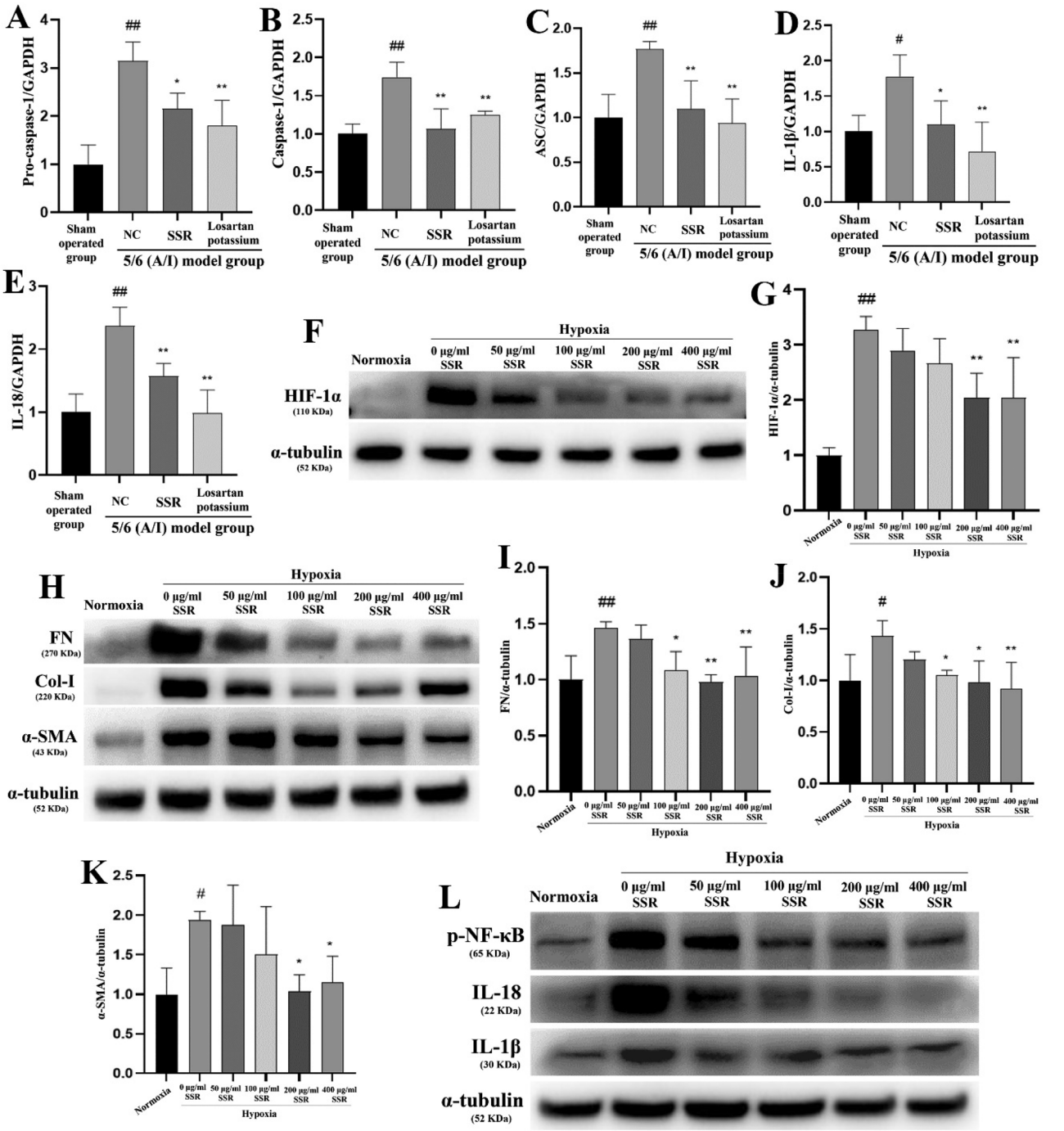

Figure 6. Shen Shuai II Recipe (SSR) suppresses NLRP3 inflammasome activation and fibrosis signaling in CKD models. (A) to (E) Western blot results of the effect of SSR on the expression of NLRP3, pro-caspase-1, caspase-1, ASC, IL-1β and IL-18 in 5/6 (A/I) rats. #: Compared with the sham-operated group, #$p < .05$, ##$p < .01$.*: Compared with the NC group, *$p < .05$, **$p < .01$. (F) and (G) Western blot results of the effect of SSR on the expression of HIF-1α in hypoxia HK-2 cells. #: Compared with the normoxia group, ##$p < .01$.*: Compared with the 0 μg/ml group, **$p < .01$. Protein bands: HIF-1α (1:2000, 110 KDa), α-tubulin (1:2000, 52 KDa). (H) to (K) Western blot results of the effect of SSR on the expression of FN, α-SMA and Col-I in hypoxia HK-2 cells. #: Compared with the normoxia group, #$p < .05$, ##$p < .01$.*: Compared with the 0 μg/ml group, *$p < .05$, **$p < .01$. Protein bands: FN (1:2000, 270 KDa), Col-I (1:2000, 220 KDa), α-SMA (1:1000, 43 KDa), α-tubulin(1:2000,52 KDa). (L) Western blot results of the effect of SSR on the expression of p-NF-κB, IL-1β, and IL-18 in hypoxia HK-2 cells. Protein bands: P-NF-κB (1:1000, 65 KDa), IL-1β (1:1000, 30 KDa), IL-18 (1:1000, 22 KDa), α-tubulin (1:2000, 52 KDa).

treatment synergistically enhanced the reduction of these markers ($p < .05$), except for Col-I ($p > .05$) (Figures 7(G–N) and 8(A–D)). These results confirm that SSR ameliorates hypoxia-induced fibrosis by targeting NLRP3 inflammasome activation, aligning with its efficacy observed in the 5/6 nephrectomy (A/I) rat model. The synergistic interaction underscores NLRP3 as a critical mediator of SSR's anti-inflammatory and anti-fibrotic effects, providing mechanistic evidence that dual-pathway inhibition more effectively disrupts fibrotic signaling cascades.

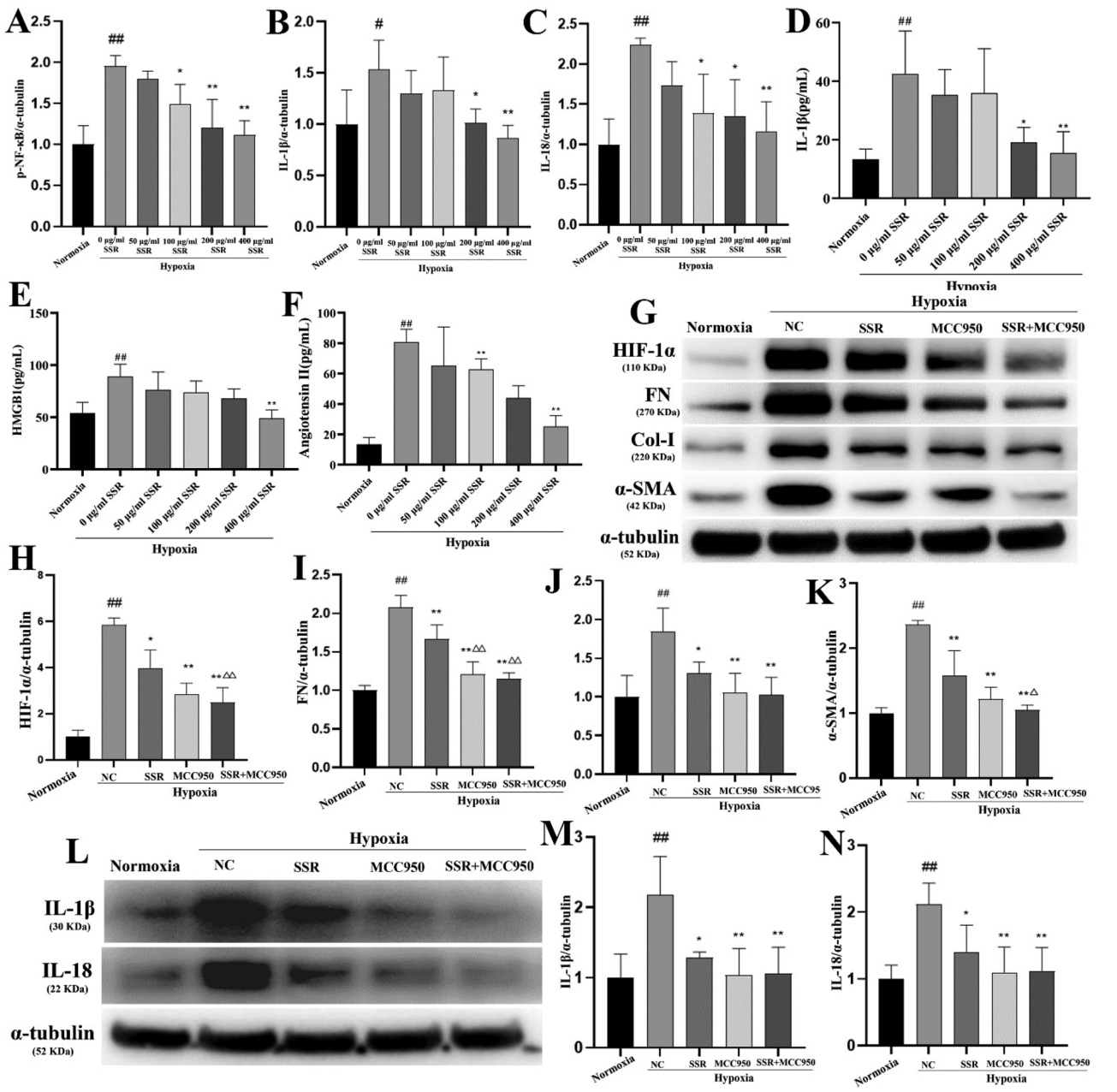

Figure 7. SSR synergizes with MCC950 to suppress hypoxia-driven inflammatory and fibrotic markers in HK-2 cells (A) to (C) Western blot results of the effect of SSR on the expression of p-NF-κB, IL-1β and IL-18 in hypoxia HK-2 cells. #: Compared with the normoxia group, #$p<.05$, ##$p<.01$.*: Compared with the 0 μg/ml group, *$p<.05$, **$p<.01$. (D) The levels of IL-1β in the culture medium of HK-2 cells treated with SSR. #: Compared with the normoxia group, ##$p<.01$.*: Compared with the 0 μg/ml group, *$p<.05$, **$p<.01$. (E) The levels of HMGB1 in the culture medium of HK-2 cells treated with SSR. #: Compared with the normoxia group, ##$p<.01$.*: Compared with the 0 μg/ml group, **$p<.01$. (F) The levels of Ang-II in the culture medium of HK-2 cells treated with SSR. #: Compared with the normoxia group, ##$p<.01$.*: Compared with the 0 μg/ml group, **$p<.01$. (G) to (K) Western blot results of the effect of SSR and MCC950 on the expression of HIF-1α, FN, α-SMA and Col-I in hypoxia HK-2 cells. #: Compared with the normoxia group, ##$p<.01$.*: Compared with the NC group, *$p<.05$, **$p<.01$. Compared with hypoxia + SSR group, △$p<.05$, △△$p<.01$. Protein bands: HIF-1α (1:2000, 110 KDa), FN (1:2000, 270 KDa), col-I (1:2000, 220 KDa), α-SMA (1:1000, 43KDa), α-tubulin(1:2000, 52 KDa). (L) to (N) Western blot results of the effect of SSR and MCC950 on the expression of IL-1β and IL-18 in hypoxia HK-2 cells. #: Compared with the normoxia group, ##$p<.01$.*: Compared with the NC group, *$p<.05$, **$p<.01$. NC: negative control. MCC950: Selective inhibitor of NLRP3 inflammasome. Protein bands: IL-1β (1:1000, 30 KDa), IL-18 (1:1000, 22 KDa), α-tubulin(1:2000, 52 KDa).

SSR ameliorates inflammation-induced fibrosis by suppressing the NLRP3 inflammasome via modulation of the TLR4/MyD88/NF-κB pathway

In the 5/6 nephrectomy (A/I) rat model, renal tissues exhibited significantly elevated expression of TLR4 ($F=31.83$, $p<.0001$), MyD88 ($F=23.82$, $p<.0001$) and p-NF-κB ($F=7.512$, $p<.01$) proteins compared to sham-operated group. SSR treatment markedly reduced these proteins (Figure 8(E–H)), indicating its capacity to inhibit TLR4/MyD88/NF-κB pathway activation.

To further validate the mechanism, MyD88 siRNA was transfected into HK-2 cells. Compared to the hypoxia group, MyD88

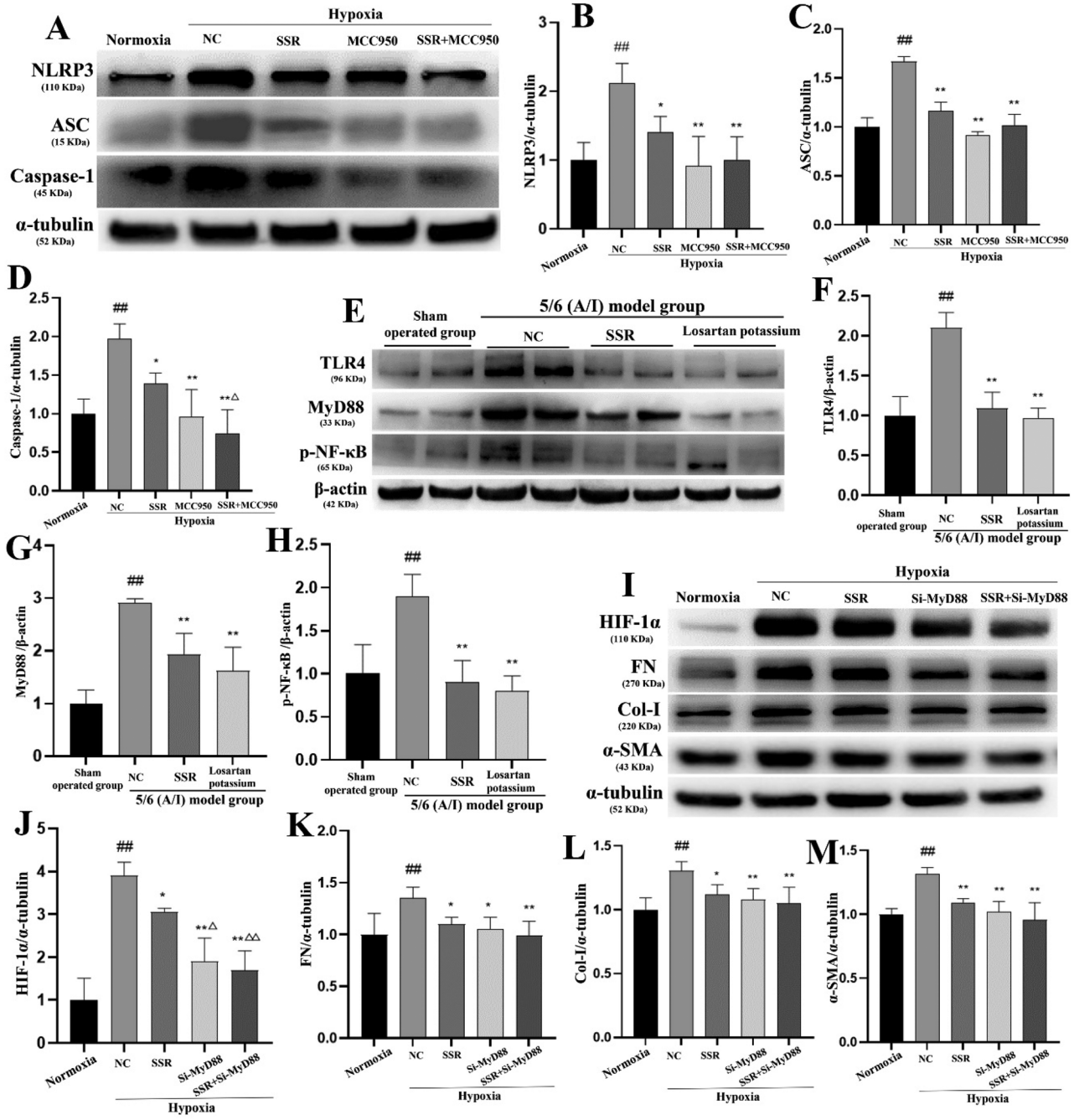

Figure 8. SSR synergizes with MCC950 and MyD88 siRNA to suppress NLRP3 inflammasome and TLR4/MyD88/NF-κB signaling. (A) to (D) Western blot results of the effect of SSR and MCC950 on the expression of NLRP3, caspase-1 and ASC in hypoxia HK-2 cells. #: Compared with the normoxia group, ##$p<.01$.*: Compared with the NC group, *$p<.05$, **$p<.01$. NC: negative control. Protein bands: NLRP3 (1:1000, 110 KDa), caspase-1 (1:2000, 45 KDa), ASC (1:1000, 15 KDa), α-tubulin (1:2000, 52 KDa). (E) to (H) Western blot results of the effect of SSR on the expression of TLR4, MyD88, and P-NF-κB in 5/6 (A/I) rats. #: Compared with the sham-operated group, ##$p<.01$.*: Compared with the NC group, **$p<.01$. Protein bands: TLR4 (1:1000, 96 KDa), MyD88 (1:2000, 33KDa), P-NF-κB (1:1000, 65KDa), β-actin (1:2000, 42 KDa). (I) to (M) Western blot results of the effect of SSR and MyD88siRNA on the expression of HIF-1α, FN, α-SMA and Col-I in hypoxia HK-2 cells. #: Compared with the normoxia group, ##$p<.01$.*: Compared with the NC group, *$p<.05$, **$p<.01$. NC: negative control. Protein bands: HIF-1α (1:2000, 110 KDa), FN (1:2000, 270 KDa), Col-I (1:2000, 220 KDa), α-SMA (1:1000, 43 KDa), α-tubulin (1:2000, 52 KDa).

siRNA significantly decreased the expression of HIF-1α($F=30.64$, $p<.0001$), TLR4($F=23.09$, $p<.0001$), MyD88($F=18.88$, $p<.0001$), p-NF-κB($F=30.43$, $p<.0001$), NLRP3($F=42.57$, $p<.0001$), caspase-1($F=66.21$, $p<.0001$), ASC($F=22.87$, $p<.0001$), IL-1β($F=21.59$, $p<.0001$), IL-18($F=30.67$, $p<.0001$), TNF-α($F=27.21$, $p<.0001$), Col-I($F=6.335$, $p<.01$), FN ($F=5.165$, $p<.01$)and α-SMA ($F=13.55$, $p<.0001$) (Figures 8(I–M) and 9(A–L)). IL-1β immunofluorescence corroborated reduced inflammatory factor expression (Figure 9(M)). These results suggest that inhibiting the TLR4/MyD88/NF-κB pathway not only alleviates hypoxia but also suppresses NLRP3 inflammasome activation, fibrosis, and inflammation in HK-2 cells. Notably, combined SSR and MyD88 siRNA treatment synergistically suppressed TLR4/MyD88/NF-κB pathway-related proteins (TLR4, MyD88 and p-NF-κB) and NLRP3 inflammasome-

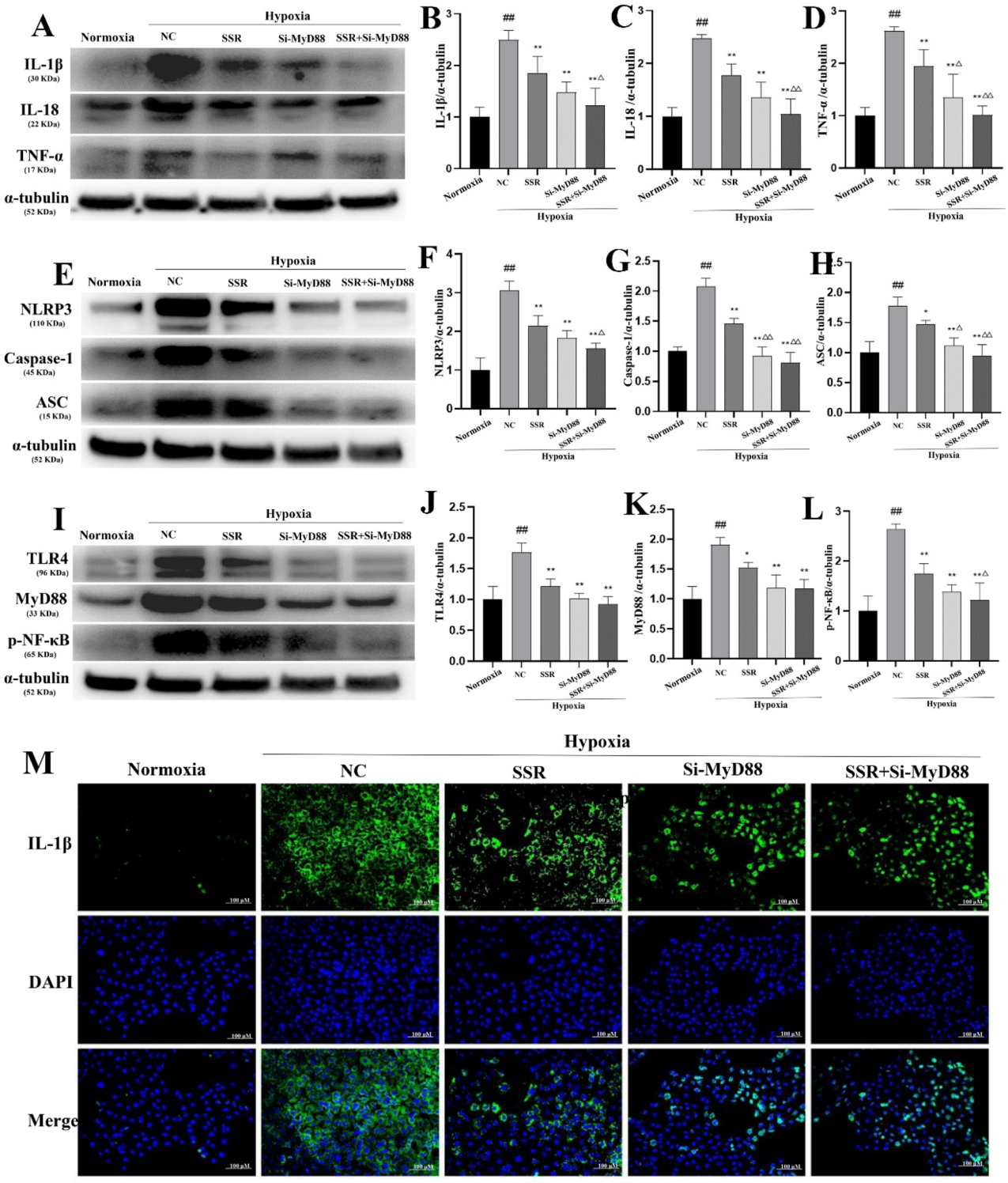

Figure 9. Synergistic inhibition of inflammatory and fibrotic pathways by SSR and MyD88 siRNA in hypoxic HK-2 cells. (A) to (D) Western blot results of the effect of SSR and MyD88siRNA on the expression of IL-1β, IL-18 and TNF-α and in hypoxia HK-2 cells. #: Compared with the normoxia group, ##$p < .01$.*: Compared with the NC group, *$p < .05$, **$p < .01$. Compared with hypoxia + SSR group, △$p < .05$, △△$p < .01$. Protein bands: IL-1β (1:1000, 30KDa), IL-18 (1:1000, 22KDa), TNF-α (1:1000, 17KDa), α-tubulin (1:2000, 52 KDa). (E) to (H) Western blot results of the effect of SSR and MyD88siRNA on the expression of NLRP3, caspase-1 and ASC and in hypoxia HK-2 cells induced by hypoxia. #: Compared with the normoxia group, ##$p < .01$.*: Compared with the NC group, *$p < .05$, **$p < .01$. Compared with hypoxia + SSR group, △$p < .05$, △△$p < .01$. Protein bands: NLRP3 (1:1000, 110 KDa), caspase-1 (1:2000, 45 KDa), ASC (1:1000, 15 KDa), α-tubulin (1:2000, 52 KDa). (I) to (L) Western blot results of the effect of SSR and MyD88siRNA on the expression of TLR4、MyD88 and P-NF-κB and in hypoxia HK-2 cells. #: Compared with the normoxia group, ##$p < .01$.*: Compared with the NC group, *$p < .05$, **$p < .01$. Compared with hypoxia + SSR group, △$p < 0.05$. Protein bands: TLR4 (1:1000, 96 KDa), MyD88 (1:2000, 33 KDa), P-NF-κB (1:1000, 65 KDa), α-tubulin (1:2000, 52 KDa). (M) Immunofluorescence staining of IL-1β (green) and DAPI (blue) in HK-2 cells induced by hypoxia. NC: negative control. Scale bar: 100 μm.

related proteins (NLRP3, caspase-1 and ASC) more effectively than either intervention alone ($p < .01$ or $p < .05$) (Figure 9(E–L)). These findings establish that SSR disrupts NLRP3 inflammasome activation by targeting the upstream TLR4/MyD88/NF-κB, thereby mitigating hypoxia-driven inflammation and fibrosis.

Discussion

Hypoxia-induced kidney injury is a pivotal driver of chronic kidney disease (CKD) progression, with proximal tubular epithelial cells being particularly vulnerable due to their elevated mitochondrial density and oxygen dependency [5]. Our previous studies have demonstrated that progressive declines in renal oxygenation and blood flow during CKD advancement [18], alongside pronounced HIF-1α expression in damaged tubules of 5/6 nephrectomy (A/I) model [15], underscoring hypoxia's central role in CKD pathogenesis. Hypoxia drives the secretory phenotypic transformation of renal tubular epithelial cells [19], reprograms inflammatory transcription, and accelerates fibrogenesis, thereby initiating a self-perpetuating cycle of hypoxia-inflammation-fibrosis [20]. Notably, hypoxic injury activates innate immune responses, accelerating renal tubulointerstitial fibrosis, which is not only a pathological feature of CKD but also a key initiating factor and independent risk factor for fibrosis progression [9]. Earlier observations revealed the macrophage marker F4/80 was highly expressed in the renal tubule interstitium of 5/6 (A/I) rats, colocalizing with HIF-1α and α-SMA [15,16], highlighting the triad of hypoxia, inflammation, and fibrosis. In this study, elevated HIF-1α expression in both the 5/6 (A/I) rat model and hypoxic HK-2 cells reaffirmed t hypoxia as a unifying mechanism linking inflammation and fibrosis. SSR treatment ameliorated hypoxia and improved renal function, consistent with previous findings [14–17]. However, the precise mechanisms by which SSR exerts its effects remain to be fully elucidated. Hypoxia and fibrosis activate multiple signaling pathways that promote fibroblast proliferation, ECM deposition, oxidative stress and noninfectious inflammation [21]. SSR has been shown to mitigate these processes by improving renal oxygenation, reducing inflammatory cell infiltration and suppressing fibrosis markers such as Col-I, FN, and α-SMA [14–17]. In this study, SSR significantly reduced HIF-1α, fibrosis markers and inflammatory factors (p-NF-κB, IL-1β, and IL-18) in both hypoxic HK-2 cells and 5/6 (A/I) rats, demonstrating its concentration-dependent anti-fibrotic and anti-inflammatory effects. These findings extend prior work by mechanistically linking SSR's hypoxia-alleviating properties to downstream pathway modulation, thereby addressing a critical knowledge gap in traditional Chinese medicine (TCM) interventions for CKD.

The NLRP3 inflammasome, a pivotal mediator of inflammation- driven fibrosis, has emerged as a promising therapeutic target in CKD [22]. Chronic hypoxia activates NLRP3 inflammasome, resulting in the secretion of IL-1β and IL-18, both of which significantly exacerbate fibrotic processes [23]. In our study, SSR treatment markedly suppressed hypoxia-induced upregulation of NLRP3, caspase-1, ASC, IL-1β, and IL-18 in 5/6 (A/I) rats, demonstrating its potent anti-fibrotic activity. Combined of SSR with MCC950 synergistically attenuated fibrosis, confirmed NLRP3 suppression as a key mechanism underlying SSR's efficacy. Furthermore, TLR4, a pattern recognition receptor expressed in renal tubular epithelial cells, was identified as a central regulator of hypoxia-driven fibrosis [10]. The TLR4/MyD88/NF-κB axis serves as a critical upstream regulator of NLRP3 inflammasome activation. Under hypoxic conditions, DAMPs such as HMGB1 and Ang II bind to TLR4, initiating MyD88-dependent recruitment of IRAK kinases, which subsequently phosphorylate IκBα to release NF-κB. Activated NF-κB drives the transcription of pro-inflammatory cytokines (IL-1β, TNF-α) and primes NLRP3 and pro-IL-1β expression [24,25]. Our data showed that SSR downregulated both TLR4/MyD88/NF-κB signaling and NLRP3 inflammasome components (NLRP3, ASC, caspase-1), indicating that SSR disrupts the crosstalk between these pathways. The synergistic effect of SSR with MCC950 further supports the interdependence of these pathways in fibrosis progression. Beyond suppressing DAMPs, SSR may directly target key nodes within the TLR4/MyD88/NF-κB/NLRP3 axis. MyD88 homodimerization is essential for signal transduction, and natural compounds have been reported to inhibit MyD88 oligomerization or its interaction with TLR4 [26]. Our MyD88 siRNA experiments, which phenocopied SSR's effects, suggest that SSR may impair MyD88 recruitment or stability. Additionally, SSR's reduction of p-NF-κB implies potential inhibition of IKKβ activity or stabilization of IκBα, limiting NF-κB nuclear translocation. Future studies should explore whether SSR modulates post-translational modifications to suppress this pathway.

Ang II and HMGB1 act as classical damage-associated molecular patterns (DAMPs), activating TLRs on cell surfaces. MyD88, a key adaptor protein, bridges TLR signaling with the IL-1 cytokine family receptor pathway, facilitating upstream to downstream signal transduction [27]. IL-1 receptor-associated kinase (IRAK), through its interaction with MyD88, modulates cell energy metabolism and the cell cycle [28]. In hypoxic-ischemic renal injury, IL-1β binds to the IL-1 receptor triggers MyD88 activation *via* intracellular IRAK4, stabilizing c-Myc expression and promoting ECM overproduction [29]. MyD88 homodimerization inhibitors, such as TJ-M2010-2, have been shown to suppress TRAF6, p65, and Snail expression, inhibiting EMT and fibrosis in renal injury models [30]. In this study, hypoxia-induced upregulation of TLR4, MyD88, and p-NF-κB was significantly attenuated by SSR treatment, mirroring the effects of MyD88 siRNA. These findings suggest that SSR inhibits the TLR4/MyD88/NF-κB axis, consequently suppressing NLRP3 inflammasome activation and fibrosis progression.

Unlike synthetic inhibitors targeting single molecules (TAK-242 for TLR4 or MCC950 for NLRP3) [31,32], SSR's multi-component nature enables simultaneous inhibition of both upstream (TLR4/MyD88/NF-κB) and downstream (NLRP3) pro-fibrotic signals. This polypharmacological action aligns with traditional Chinese medicine's holistic therapeutic strategy, offering a broader therapeutic window compared to

single-target agents. For instance, concurrent suppression of NF-κB-driven cytokine priming and NLRP3-mediated pyroptosis may more effectively halt fibrosis progression, as inflammasome activation requires both signals [24]. These findings extend previous reports on SSR's anti-fibrotic effects [13–17] by mechanistically linking hypoxia amelioration to TLR4/MyD88/NF-κB/NLRP3 pathway inhibition.

Our findings demonstrate that SSR alleviates renal fibrosis by improving hypoxia and inhibiting the TLR4/MyD88/NF-κB/NLRP3 pathway, thereby suppressing inflammation and fibrosis. While MyD88 knockdown confirmed the pathway's role in SSR's effects, future studies with TLR4 overexpression could provide additional mechanistic insight. However, the consistency of our pharmacological and genetic inhibition data across multiple pathway nodes strongly supports our conclusions. Nevertheless, several translational challenges must be addressed to advance SSR's clinical development. As a multi-component herbal formulation, SSR's efficacy may depend on synergistic interactions among its bioactive constituents, yet variability in the bioavailability of individual components due to solubility limitations or first-pass metabolism could influence clinical outcomes. Although our dose selection (in rats and *in vitro*) was based on prior optimization studies [14,17], translating these findings to human applications necessitates rigorous determination of effective and safe dosage ranges, particularly to mitigate risks of herb-drug interactions with standard CKD treatments such as RAS inhibitors. Furthermore, while no adverse effects were observed in SSR-treated rats over eight weeks, long-term safety assessments in higher species and human trials are essential to confirm tolerability. These challenges highlight the need for interdisciplinary collaboration to bridge preclinical promise and clinical utility.

In conclusion, our study provides a foundation for SSR's application in CKD, with future work focusing on pharmacokinetic profiling and early-phase clinical trials.

Acknowledgements

We thank Shanghai Ordovician Biotechnology Co., LTD. for providing the rat modeling guidance. And the authors declare that there are no conflicts of interest with Shanghai Ordovician Biotechnology Co., LTD in this work.

Ethical approval

All animal experiments were approved by the Experimental Animal Administration Committee of Shanghai University of Traditional Chinese Medicine, and the animal ethics registration number was No. SZY201604006.

Author contributions

ZY and WC conceived and designed the study. ZY, ZL, WM, XL, and LTT performed the experimental work and analyzed the results. ZY and ZL wrote the paper. ZY and WC edited and revised. All authors agree to be accountable for all aspects of work ensuring integrity and accuracy.

Disclosure statement

No potential conflict of interest was reported by the author(s).

Funding

The study was supported by National Natural Science Foundation of China (82405247), National Natural Science Foundation of China (81973770), National Natural Science Foundation of China (82174289), Foundation of Shanghai Municipal Health Commission Planning (20214Y0382), Shanghai Tree-Year Project of Traditional Chinese Medicine (ZY [2018-2020]-FWTX-7005), Key Disciplines Group Construction Project of Pudong Health Bureau of Shanghai (PWZxq2017-07). 2025 Pudong New Area Distinguished TCM Practitioner Studios Construction Project (NO.PDZY-2025-0704).

References

[1] Deng Y, Li N, Wu Y, et al. Global, regional, and national burden of diabetes-related chronic kidney disease from 1990 to 2019. Front Endocrinol. 2021;12:672350. doi: 10.3389/fendo.2021.672350.

[2] Harada R, Hamasaki Y, Okuda Y, et al. Epidemiology of pediatric chronic kidney disease/kidney failure: learning from registries and cohort studies. Pediatr Nephrol. 2022; 37(6):1215–1229. doi: 10.1007/s00467-021-05145-1.

[3] Szlagor M, Dybiec J, Młynarska E, et al. Chronic kidney disease as a comorbidity in heart failure. Int J Mol Sci. 2023;24(3):2988. doi: 10.3390/ijms24032988.

[4] Wei X, Hou Y, Long M, et al. Advances in energy metabolism in renal fibrosis. Life Sci. 2023;312:121033. doi: 10.1016/j.lfs.2022.121033.

[5] Wang B, Li Z-L, Zhang Y-L, et al. Hypoxia and chronic kidney disease. EBioMedicine. 2022;77:103942. doi: 10.1016/j.ebiom.2022.103942.

[6] Zhu Z, Hu J, Chen Z, et al. Transition of acute kidney injury to chronic kidney disease: role of metabolic reprogramming. Metabolism. 2022;131:155194. doi: 10.1016/j.metabol.2022.155194.

[7] Schnaper HW. The tubulointerstitial pathophysiology of progressive kidney disease. Adv Chronic Kidney Dis. 2017;24(2):107–116. doi: 10.1053/j.ackd.2016.11.011.

[8] Abumoawad A, Saad A, Ferguson CM, et al. Tissue hypoxia, inflammation, and loss of glomerular filtration rate in human atherosclerotic renovascular disease. Kidney Int. 2019;95(4):948–957. doi: 10.1016/j.kint.2018.11.039.

[9] Li Z-L, Liu B-C. Hypoxia and renal tubulointerstitial fibrosis. Adv Exp Med Biol. 2019;1165:467–485. doi: 10.1007/978-981-13-8871-2_23.

[10] Duan T, Du Y, Xing C, et al. Toll-like receptor signaling and its role in cell-mediated immunity. Front Immunol. 2022;13:812774. doi: 10.3389/fimmu.2022.812774.

[11] Chen D, Sui L, Chen C, et al. Atorvastatin suppresses NLRP3 inflammasome activation in intracerebral hemorrhage via TLR4- and MyD88-dependent pathways. Aging. 2022;14(1):462–476. doi: 10.18632/aging.203824.

[12] Ciesielska A, Matyjek M, Kwiatkowska K. TLR4 and CD14 trafficking and its influence on LPS-induced pro-inflammatory signaling. Cell Mol Life Sci. 2021;78(4):1233–1261. doi: 10.1007/s00018-020-03656-y.

[13] Wang M, Wang L, Zhou Y, et al. Shen Shuai II Recipe attenuates renal fibrosis in chronic kidney disease by improving hypoxia-induced the imbalance of mitochondrial dynamics via PGC-1α activation. Phytomedicine. 2022;98:153947. doi: 10.1016/j.phymed.2022.153947.
[14] Yang L, Wang M, Zhou Y, et al. Shen Shuai II Recipe attenuates renal interstitial fibrosis by improving hypoxia via the IL-1β/c-Myc pathway. Evid Based Complement Alternat Med. 2021;2021:5539584. doi: 10.1155/2021/5539584.
[15] Wang M, Yang J, Zhou Y, et al. Shen Shuai II Recipe attenuates apoptosis and renal fibrosis in chronic kidney disease by increasing renal blood flow and improving oxygen consumption. Evid Based Complement Alternat Med. 2018;2018(1):7602962. doi: 10.1155/2018/7602962.
[16] Wang M, Yang L, Yang J, et al. Shen Shuai II Recipe attenuates renal injury and fibrosis in chronic kidney disease by regulating NLRP3 inflammasome and Sirt1/Smad3 deacetylation pathway. BMC Complement Altern Med. 2019;19(1):107. doi: 10.1186/s12906-019-2524-6.
[17] Wang M, Yang J, Wang C. Shen Shuai II Recipe attenuates apoptosis in 5/6 renal ablation/infarction rats by inhibiting p53 and the mitochondrial pathway of apoptosis. Oxid Med Cell Longev. 2020;2020:7083575. doi: 10.1155/2020/7083575.
[18] Yang J, Yang S, Xu Y, et al. Evaluation of renal oxygenation and hemodynamics in patients with chronic kidney disease by blood oxygenation level-dependent magnetic resonance imaging and intrarenal doppler ultrasonography. Nephron. 2021;145(6):653–663. doi: 10.1159/000516637.
[19] Chen B, Brem AS, Gong R. The Janus view: dual roles for hypoxia-inducible factor in renal repair after acute kidney injury. Am J Physiol Renal Physiol. 2022;323(1):F1–F3. doi: 10.1152/ajprenal.00130.2022.
[20] Cai J, Hu M, Chen Z, et al. The roles and mechanisms of hypoxia in liver fibrosis. J Transl Med. 2021;19(1):186. doi: 10.1186/s12967-021-02854-x.
[21] Liu M, Ning X, Li R, et al. Signalling pathways involved in hypoxia-induced renal fibrosis. J Cell Mol Med. 2017;21(7):1248–1259. doi: 10.1111/jcmm.13060.
[22] Mulay SR. Multifactorial functions of the inflammasome component NLRP3 in pathogenesis of chronic kidney diseases. Kidney Int. 2019;96(1):58–66. doi: 10.1016/j.kint.2019.01.014.
[23] Bai C, Zhu Y, Dong Q, et al. Chronic intermittent hypoxia induces the pyroptosis of renal tubular epithelial cells by activating the NLRP3 inflammasome. Bioengineered. 2022;13(3):7528–7540. doi: 10.1080/21655979.2022.2047394.
[24] Huang G, Zhang Y, Zhang Y, et al. Chronic kidney disease and NLRP3 inflammasome: pathogenesis, development and targeted therapeutic strategies. Biochem Biophys Rep. 2023;33:101417. doi: 10.1016/j.bbrep.2022.101417.
[25] Teh HX, Phang SJ, Looi ML, et al. Molecular pathways of NF-κB and NLRP3 inflammasome as potential targets in the treatment of inflammation in diabetic wounds: a review. Life Sci. 2023;334:122228. doi: 10.1016/j.lfs.2023.122228.
[26] Kuzmich NN, Sivak KV, Chubarev VN, et al. TLR4 signaling pathway modulators as potential therapeutics in inflammation and sepsis. Vaccines. 2017;5(4):34. doi: 10.3390/vaccines5040034.
[27] Chen L, Zheng L, Chen P, et al. Myeloid differentiation primary response protein 88 (MyD88): the central hub of TLR/IL-1R signaling. J Med Chem. 2020;63(22):13316–13329. doi: 10.1021/acs.jmedchem.0c00884.
[28] Yang J, Liu D-J, Zheng J-H, et al. IRAK2-NF-κB signaling promotes glycolysis-dependent tumor growth in pancreatic cancer. Cell Oncol. 2022;45(3):367–379. doi: 10.1007/s13402-022-00670-z.
[29] Lemos DR, McMurdo M, Karaca G, et al. Interleukin-1β activates a MYC-dependent metabolic switch in kidney stromal cells necessary for progressive tubulointerstitial fibrosis. J Am Soc Nephrol. 2018;29(6):1690–1705. doi: 10.1681/ASN.2017121283.
[30] Liu J-H, He L, Zou Z-M, et al. A novel inhibitor of homodimerization targeting MyD88 ameliorates renal interstitial fibrosis by counteracting TGF-β1-induced EMT in vivo and in vitro. Kidney Blood Press Res. 2018;43(5):1677–1687. doi: 10.1159/000494745.
[31] Babuta M, Morel C, de Carvalho Ribeiro M, et al. Neutrophil extracellular traps activate hepatic stellate cells and monocytes via NLRP3 sensing in alcohol-induced acceleration of MASH fibrosis. Gut. 2024;73(11):1854–1869. doi: 10.1136/gutjnl-2023-331447.
[32] Xia Y-M, Guan Y-Q, Liang J-F, et al. TAK-242 improves sepsis-associated acute kidney injury in rats by inhibiting the TLR4/NF-κB signaling pathway. Ren Fail. 2024;46(1):2313176. doi: 10.1080/0886022X.2024.2313176.